

Battery-time-space fragment-based formulation for the Electric Autonomous Dial-a-Ride Problem

Boshuai Zhao*

Université Paris-Saclay, CentraleSupélec, Laboratoire Génie Industriel, France

boshuai.zhao@centralesupelec.fr; zhaoboshuai1995@163.com

Adam Abdin

Université Paris-Saclay, CentraleSupélec, Laboratoire Génie Industriel

adam.abdin@centralesupelec.fr

Jakob Puchinger

EM Normandie Business School, Métis Lab, France

Université Paris-Saclay, CentraleSupélec, Laboratoire Génie Industriel

jakob.puchinger@centralesupelec.fr

January 8, 2026

Abstract: The Electric Autonomous Dial-A-Ride Problem (E-ADARP) optimizes routing and scheduling for electric autonomous vehicles to transport customers from origins to destinations. It features a combined objective that minimizes travel cost and excess user ride time, and allows partial recharging. Motivated by practical scenarios where time and battery data are available with limited precision, we introduce a discrete variant of the problem, termed D-E-ADARP, in which all time and battery parameters are discretized. This enables the development of our alternative solution approach: the discrete battery-time-space fragment-based formulation (BTSFF). In this framework, a fragment represents a subpath with an associated cost that accounts for both travel cost and excess user ride time. The BTSFF network integrates spatial, temporal, and battery dimensions, with the latter two discretized into finite indices. Computational results show that BTSFF solves D-E-ADARP significantly more efficiently than existing methods applied to the original E-ADARP. In addition, BTSFF efficiently provides high-quality lower bounds for E-ADARP and accelerates solving its battery

swap variants. For E-ADARP, a relaxed network is constructed by rounding down travel times and battery consumptions, enabling a valid lower bound. For battery swap variants, BTSFF integrates lazy constraints via callbacks to correct time discretization errors, guaranteeing optimal solutions. Experiments show BTSFF outperforms benchmark methods in efficiency.

Keywords: Electric autonomous dial-a-ride problem, Fragment, Discretization

1 Background

The Dial-a-Ride Problem (DARP) involves designing vehicle routes and schedules to transport passengers from their origins to destinations while minimizing travel cost. The Electric Autonomous Dial-a-Ride Problem (E-ADARP) extends DARP by considering fleets of electric, self-driving vehicles. The new setting imposes additional operational constraints due to limited battery capacity, while eliminating those associated with human drivers (e.g., maximum driving time). The need for recharging further increases complexity, requiring decisions about when, where, and how much to recharge—decisions that must balance energy needs with charging time. Additionally, the objective function is more complex, as it not only minimizes travel cost but also accounts for excess user ride time. Both the new constraints and the bi-objective nature further increase computational complexity by adding decision variables and expanding the solution space.

DARP and E-ADARP have a wide range of application domains, including food delivery (e.g., Meituan, Uber Eats, Deliveroo), passenger transport (e.g., DiDi, Uber), non-emergency patient transfers, campus shuttle services, and tourist transportation. While many studies have provided a formal definition and conducted in-depth investigations of E-ADARP (e.g., Bongiovanni et al. (2019); Su et al. (2024)), they typically assume scenarios in which time and battery parameters are highly precise or nearly continuous. For instance, on-demand services such as ride-hailing or food delivery typically require minute- or even second-level accuracy, which motivates the use of continuous-time modeling in existing studies.

Nevertheless, we observe that many real-world applications naturally involve discretized time and battery parameters. In particular, scenarios such as non-emergency patient transfers, campus shuttle services, and tourist transportation often operate with coarser scheduling granularity—typically at 5- or 10-minute intervals—due to lower urgency or operational constraints. In such cases, a full-day planning horizon (24 hours) results in a manageable number of time indices, typically ranging from 144 (10-minute intervals) to 288 (5-minute intervals). Similarly, in short-horizon applications such as drone delivery, the planning window often spans only 2–4 hours, with battery typically lasting 30 to 60 minutes. Even

with minute-level granularity, this yields approximately 120–240 time steps and 30–60 battery levels, which are comparable in scale to the coarser-time cases discussed above. Similar levels of time and battery discretization have been adopted in various vehicle routing problem studies (Mahmoudi & Zhou, 2016; Fernández et al., 2022; Bruni et al., 2025), as further discussed in Section 2.2.

The above observation indicates that discrete representations naturally arise in practice regardless of the specific granularity of each scenario. Evidence from various application settings also suggests that the resulting time and battery discretizations remain computationally manageable. Building on these insights, we define a discrete variant of E-ADARP with discrete time and battery parameters, referred to as the Discrete Electric Autonomous Dial-a-Ride Problem (D-E-ADARP).

Our motivation to focus on D-E-ADARP is primarily methodological. Traditional methods, such as branch-and-cut (Cordeau, 2006) and branch-and-price (Ropke & Cordeau, 2009; Baldacci et al., 2011), have been widely used to solve DARP and can also be applied to E-ADARP. More recently, Rist & Forbes (2021) introduce a fragment-based formulation for the DARP that significantly outperforms existing methods. In this context, a “fragment” refers to a partial path characterized by an empty load at both the start and end nodes. This approach appears to establish a new category of methods. However, partial recharging and continuous battery indices in E-ADARP limit the straightforward application of fragment-based formulations used in DARP, since the resulting complex time schedules cannot be effectively managed through the lazy-constraint callback, as in Rist & Forbes (2021). Although some studies have introduced fragment-based ideas for E-ADARP, their potential has not been fully realized. For instance, Su et al. (2023) integrated the fragment concept into a branch-and-price (B&P) framework, where fragments rather than nodes serve as the basis for subproblem path generation. By contrast, D-E-ADARP, with its discretized time and battery indices, enables the use of discretization techniques that circumvent the challenges posed by continuous-parameter settings in E-ADARP.

The limited exploration of fragment methods in existing studies, together with the discrete characteristics of the D-E-ADARP, motivates us to design a tailored discretized fragment-based method for the (D-)E-ADARP. This leads to our primary question: can discrete solution methods, explicitly designed for the D-E-ADARP, achieve superior performance compared to approaches originally developed for E-ADARP? To address this question, we propose the Battery–Time–Space Fragment-Based Formulation (BTSFF). BTSFF leverages fragments to provide a compact and tractable representation of partial paths within a battery–time–space network, which augments the physical network with two additional dimensions: time and battery. Beyond serving as a solution method, we also examine whether BTSFF can provide lower bounds for the original E-ADARP. For continuous time

and battery parameters, we construct a relaxed network by rounding down arc consumptions, which may produce infeasible solutions but still valid lower bounds. We further analyze how the granularity of discretization affects both computational efficiency and bound quality.

Meanwhile, battery swapping has become increasingly relevant in E-ADARP as the technology gains wider adoption, and similar trends are observed with the emergence of ultra-fast charging systems. For example, BYD recently introduced a system capable of fully charging an EV within five minutes (BYD Auto, 2025), making fast charging comparable to swapping in speed. Motivated by these developments, we extend our study to a battery-swapping variant of E-ADARP. In this variant, we adopt discretized battery settings while maintaining continuous time (with the rationale explained in Section 3.4) and apply BTSFF together with a lazy-constraint callback to remove paths with infeasible schedules. This allows us to evaluate whether BTSFF can be effectively extended to continuous-time settings.

The main contributions of this paper are summarized as follows:

- We identify a discrete variant of the E-ADARP and develop a tailored solution method that outperforms existing approaches under reasonable time discretization.
- We show that the proposed Battery–Time–Space Fragment-Based Formulation (BTSFF) can generate high-quality lower bounds for the original E-ADARP, even under coarse time discretization (e.g., 10-minute intervals).
- We demonstrate that integrating BTSFF with a callback mechanism enables the handling of continuous-parameter settings, especially for the battery-swapping variant.

From a practical perspective, the newly defined problem and proposed method provide rapid solutions in autonomous delivery and transportation scenarios where coarse time and battery precision are acceptable. From an academic perspective, the effectiveness of BTSFF underscores the modeling potential of jointly discretizing time and battery dimensions in vehicle routing and motivates exploration of parameters that are less commonly subjected to discretization. Moreover, the integration of discretization with fragment-level representations not only facilitates solving the problem in a discrete setting but also yields strong lower bounds for the continuous setting, thereby encouraging further investigation of discrete approaches for optimization problems with continuous parameters.

The remainder of this article is organized as follows. Section 2 presents a comprehensive review of the relevant literature. Section 3 introduces the problem statement of D-E-ADARP and presents an innovative formulation, BTSFF, for it.

Section 4 details the extension of BTSFF to E-ADARP and its battery swapping variant. In Section 5, we present and discuss the computational results. Finally, Section 6 concludes the paper.

2 Literature review

In this section, we review existing studies on DARP and E-ADARP and discuss works that apply time and battery discretization in vehicle routing problems.

2.1 Electric autonomous dial-a-ride problem

Before introducing E-ADARP, we first review a recent line of research on the DARP that centers on fragment-based methods. Alyasiry et al. (2019) are the first to propose the fragment-based approach. They apply this method to the Pickup and Delivery Problem (PDP) with Time Windows under a Last-In-First-Out (LIFO) loading constraint. PDP is a generalization of the DARP, in which multiple items from a single pickup node may be destined for different delivery nodes, and no maximum ride time constraint is imposed. In this context, fragments are defined as partial paths in which only the start and end nodes have an empty load, and the sequence adheres to the LIFO rule. Example fragment sequences include $p1p2p3d3d2d1$ and $p1p2d2p3d3d1$, where “ p ” denotes a pickup node, “ d ” denotes a delivery node, and the number indicates the customer index. This representation also applies to later parts of our study. By enumerating combinations of such fragments, the authors construct a compact formulation over a time-space network. Their computational results demonstrate the effectiveness of the approach. Importantly, this concept has also been extended beyond the strict LIFO setting. Recent studies, such as Rist & Forbes (2021), Rist & Forbes (2022), and Zhang et al. (2023), demonstrate that fragment-based methods can significantly enhance computational performance in solving DARP and its variants. In these works, fragments are not restricted to LIFO. For example, a sequence like $p1p2d1p3d2d3$ still satisfies the general fragment definition—where only the start and end nodes have an empty load. An important advantage of the fragment-based approach is that key constraints—such as pairing, precedence, capacity, time windows, and maximum ride time—are embedded during fragment generation. As a result, many DARP constraints are implicitly satisfied, reducing the burden on the main formulation. However, time-related constraints, particularly time windows and ride time limits, may still require additional handling via the time-space network or/and callback mechanisms.

Another recent line of research on the DARP introduces an event-based formulation (Gaul et al., 2022, 2024). In this formulation, each event represents

the vehicle’s state, defined by its current location, onboard customers, and the sequence of visited requests. This formulation resembles the classical arc-based one of Cordeau (2006), but instead relies on a network in which nodes represent events and arcs capture feasible transitions between them. This structure inherently satisfies pairing, precedence, and capacity constraints, thereby reducing the number of explicit constraints required in the model and enhancing computational performance.

We now turn to the development of exact algorithms for E-ADARP. In addition to the standard DARP constraints, E-ADARP has to track the vehicle’s state of charge (SoC) to determine when, where, and how much to recharge, which complicates both the routing and scheduling decisions. Bongiovanni et al. (2019) are the first to solve E-ADARP exactly, employing a branch-and-cut approach based on an arc-based formulation. Subsequently, Su et al. (2024) propose a B&P algorithm that significantly improves computational efficiency compared to Bongiovanni et al. (2019). As mentioned earlier, their approach leverages fragments as the basis for generating paths in the subproblem. More recently, Stallhofer & Parragh (2025) apply an event-based formulation to E-ADARP, extending the works of Gaul et al. (2022, 2024). With the support of additional tailored cuts, their method achieves superior performance over Su et al. (2024) on most reported benchmark instances when each recharging station is allowed to be visited at most once. However, no additional tests are provided for cases with higher visit limits.

Recent studies have explored event-based formulations for E-ADARP and incorporated fragment ideas within B&P frameworks. The best-performing approaches are the event-based method of Stallhofer & Parragh (2025) and the B&P algorithm of Su et al. (2024), with the former showing greater advantage. However, fragment-based methods have not yet been fully exploited for this problem in a direct way. Given that fragment-based approaches outperform event-based ones in the DARP, this gap motivates us to explore their more effective use in the (D-)E-ADARP.

2.2 Time and battery discretization in routing problem

Beyond exact algorithms for E-ADARP, another relevant body of work addresses the use of time and battery discretization in vehicle routing problems.

Many studies have adopted discrete time settings for modeling and optimization. For example, Santini et al. (2018) design a B&P framework to efficiently solve a feeder network design problem, which is similar to PDP. Based on real-world scenarios, they use a discrete time representation. Their computational experiments include two instances: the Baltic scenario, with a total planning horizon of one week and a time unit of two hours, and the Western African (WAF) scenario, with a four-week horizon and eight-hour time units, both corresponding to 84 time in-

dices. In addition, Mahmoudi & Zhou (2016) apply a state–space–time formulation to the PDP with time window constraints, motivated by ride-sharing applications. Their notion of “state” captures onboard customer information, which is conceptually similar to the “event” concept proposed by Gaul et al. (2022). Notably, they adopt a discrete time setting with one-minute intervals over a four-hour planning horizon, resulting in 240 time indices. Collectively, these studies adopt discrete time horizons ranging from about 80 to 240 indices.

Several studies on the Electric Vehicle Routing Problem (EVRP) adopt discretized battery settings. Fernández et al. (2022) investigate a variant of the EVRP in the context of arc routing with speed-dependent energy consumption. They demonstrate that a discretization granularity of 1000 kWs for battery capacities ranging from 25 to 75 kWh (approximately 1.3%–4% of battery capacity) offers a good trade-off between solution quality and computational tractability, and is sufficient for most case studies with negligible impact on solution quality. Bruni et al. (2025) examine the EVRP with non-linear charging functions. They state that accurately estimating battery behavior is intricate due to the presence of many uncertainties. Hence, they consider using a fine-grained discretization of 5% of battery capacity to be a reasonable choice for their study. Overall, the literature indicates that a discretization level of about 2%–5% of battery capacity is generally considered reasonable.

Many studies have considered discrete representations of either battery or time, as well as two-dimensional networks such as time–space networks. However, few studies have explored the joint discretization of both time and battery within a three-dimensional battery–time–space network, especially for routing problems similar to E-ADARP. In this work, we make the first attempt to address such a problem, aiming for a reasonable trade-off between modeling accuracy and computational tractability.

3 Problem statement and a novel formulation for D-E-ADARP

(D-)E-ADARP aims to design routes and schedules for transporting a set of customers while incorporating recharging decisions. This section begins with a formal problem description of D-E-ADARP in Section 3.1. Then, we present the construction of the battery-time-space fragment-based network and its corresponding formulation, BTSFF, in Sections 3.2 and 3.3, respectively. Finally, we present the E-ADARP variant with battery swapping.

BTSFF builds upon the frameworks proposed in Alyasiry et al. (2019), which is based on a time-space network, and Rist & Forbes (2021), which uses a physical

network representation. While we adopt the core formulation of Rist & Forbes (2021), our model extends it to a three-dimensional battery-time-space network. This network also incorporates arcs associated with charging stations.

3.1 Problem description

We first introduce the (original) E-ADARP problem description and then extend the formulation to D-E-ADARP. E-ADARP involves a total number of customers n , with each customer i having a unique pickup and delivery location pair represented as $(i, i + n)$, where i represents the pickup node and $i + n$ the corresponding delivery node. The pickup and delivery locations are represented by the sets $P = \{1, 2, \dots, n\}$ and $D = \{n + 1, n + 2, \dots, 2n\}$, respectively. The set of charging stations is denoted by S . The location set $N = P \cup D \cup S \cup \{0, 2n + 1\}$ includes all pickup and delivery locations, charging station locations, as well as the origin depot 0 and the destination depot $2n + 1$. Each location $i \in P \cup D$ is associated with a time window (e_i, l_i) , defining the earliest arrival and latest departure times. Additionally, t_{\min} and t_{\max} denote the earliest departure time from the origin depot and the latest arrival time at the destination depot, respectively. The arc set is denoted by A , including all arcs $(i, j) \in N \times N$ with $i \neq j$. For each arc $(i, j) \in A$, the minimum travel time and battery consumption are represented by C_{ij}^t , and C_{ij}^b , respectively.

The set of vehicles is denoted by V , and the parameter Q represents the vehicle load capacity. The load quantity change at location $i \in N$ is expressed as q_i , with $q_0 = q_{2n+1} = 0$ and $q_i = -q_{n+i}$ ($q_i \in \mathbb{Z}_+$) for $i \in P$. This value represents the customer demand: at pickup location $i \in P$, the vehicle increases its load by q_i , while at delivery location $i + n \in D$, it decreases the load by q_i .

Let b_{\max} denote the vehicle's maximum state of charge. The terms b_{\min} and γb_{\max} represent the minimum required SoC during the trip and before returning to the depot, respectively, where γ denotes the corresponding minimum SoC ratio. The battery charging and discharging rates per unit time are denoted by α and β , respectively.

Here, the problem has the following assumptions: first, the vehicle speed remains constant, ensuring proportionality between cost, time, distance, and battery consumption. Second, recharging is only permitted when there are no customers in the vehicle. Third, partial recharging is allowed, where the amount of battery replenished is proportional to the recharging time.

The objective of E-ADARP is to minimize a weighted cost while ensuring that no more than $|V|$ vehicles are used to serve all pickup and delivery tasks. The weighted cost consists of the total travel cost incurred by all vehicles and the total customer ride time cost, weighted by λ and $1 - \lambda$, respectively. The ride time cost is defined as the difference between each customer's actual ride time and the

corresponding direct travel time. Each vehicle starts its route at the origin depot node 0 and ends at the destination depot node $2n+1$. Before using up the battery, each vehicle is required to visit a charging station $s \in S$ to recharge. Each pickup location $i \in P$ must be visited by the same vehicle as its corresponding delivery location $i + n \in D$ (pairing), with the pickup location visited before the delivery location (precedence). Moreover, each customer $i \in P$ has a maximum ride time R_i , each location $i \in N$ has its time window, and each vehicle is limited to a capacity of at most Q .

As a notational simplification, we incorporate the service time at each location into time-related parameters and omit it explicitly throughout the paper. Following Rist & Forbes (2021), the service time at location i is embedded in both the travel time of arcs departing from i and the maximum ride time of customer i . Hence, an arc's travel time is not necessarily proportional to its travel cost, distance, or battery consumption.

Moreover, this study considers only the setting where the maximum number of allowable visits to each charging station, denoted by N_{\max} , is unlimited. This assumption is also considered in the extended scenario of Su et al. (2024). In arc-and event-based formulations, small values of N_{\max} reduce node duplication and model size, while the unlimited case is difficult to model. In contrast, BTSFF naturally handles the unlimited case without added complexity. As our focus is on general comparisons, and it is reasonable for a station to be visited unlimited times (or at least a sufficiently large number of times), we consider only the unlimited setting.

Based on the above mentioned description of E-ADARP, we define its discretized counterpart, referred to as D-E-ADARP. The key distinction lies in the use of discretized input parameters: time and battery values are quantized into predefined units. Consequently, C_{ij}^t and C_{ij}^b on all arcs are restricted to integer multiples of these units. The resulting finite sets of time indices and SoCs are denoted by T and B , respectively, for which $e_i, l_i \in T$, and $b_{\max}, b_{\min}, \gamma b_{\max} \in B$. The time horizon set $T = \{t_{\min}, t_1, t_2, \dots, t_{\max}\}$ consists of a sequence of increasingly ordered time indices, while the battery horizon set $B = \{b_{\min}, b_1, b_2, \dots, b_{\max}\}$ comprises a sequence of increasingly ordered SoCs.

3.2 Battery-time-space fragment-based network for E-ADARP

BTSFF is proposed to efficiently address E-ADARP. To clarify the design of BTSFF, we first introduce its underlying network. We begin by describing the (physical) fragment-based network used for DARP in Section 3.2.1, and then explain the battery-time-space network for D-E-ADARP in Section 3.2.2.

3.2.1 Fragment-based network for DARP

In this subsection, we largely follow the definitions of Rist & Forbes (2021).

A *DARP route* is a route $(0, i_1, i_2, \dots, i_L, 2n+1)$ for which at least one feasible schedule exists, satisfying the pairing, precedence, capacity, maximum ride time (on customers), and time window constraints of E-ADARP. Battery-related constraints are not considered at this stage. The sequence of locations (i_1, i_2, \dots, i_L) , excluding depot locations, is called a *DARP route path*. Any segment of this sequence is referred to as a route path.

A *node* is defined as a pair consisting of a location and a set of loads in the previous studies (Rist & Forbes, 2021; Zhao et al., 2025). Since we only use the fragment that only have empty loads at its start and end nodes, all nodes in this study can directly correspond to locations. Nevertheless, we retain the term “node” for consistency with previous studies.

A *fragment* refers to a partial DARP route path where only the start and end nodes have an empty load. For instance, a valid fragment could have a sequence of locations (p_1, p_2, d_2, d_1) or $(p_1, p_2, d_1, p_3, d_2, d_3)$, where p_j and d_j respectively denote the pickup and delivery locations for customer j . This style of description is also applicable throughout the entire paper. An invalid case is $(p_1, d_1, p_2, p_3, d_2, d_3)$ as this violates the empty load condition after location d_1 and should be decomposed into (p_1, d_1) and (p_2, p_3, d_2, d_3) , ensuring that a fragment starts from a pickup node and ends at a delivery node. Here, pickup and delivery nodes are simply pickup and delivery locations.

Next, we refer to the *node arc* as the connection between fragments, specifically linking a delivery node to a pickup node or the destination depot, or connecting the origin depot to a pickup node.

Building a fragment-based network involves first enumerating all feasible fragments that connect their corresponding pickup nodes to their respective delivery nodes. The network is then established by linking the origin depot with all pickup nodes, each pickup node with all delivery nodes, and all delivery nodes with the destination depot, thereby generating all the necessary node arcs. For fragment enumeration, each fragment must satisfy the E-ADARP’s constraints along its path, including the time window, maximum ride time, vehicle capacity, pairing, and precedence constraints.

Fig. 1 presents a fragment-based network for DARP. Here, ellipses represent nodes, solid lines (with ellipses on both sides) indicate fragments (its information is described above or to the right), and dashed lines with arrows signify node arcs. O^+ and O^- denote the origin and destination depots, respectively. An inherent characteristic of a feasible path is its typical initiation with a node arc extending from the origin depot to a pickup node, succeeded by a fragment from the pickup node to a delivery node. Subsequently, a node arc transition occurs

from a delivery node to a pickup node or the destination depot. This pattern persists in an alternating sequence. As illustrated in Fig. 1, dashed lines and solid lines alternate throughout any feasible path.

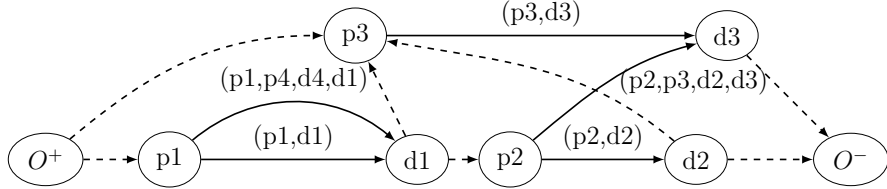


Figure 1: A fragment-based network for DARP

3.2.2 Battery-time-space fragment-based network

We now present the battery-time-space (BTS) network for E-ADARP. We begin with the generation of fragments and the calculation of their weighted costs, followed by the construction of the BTS network. In illustrating the calculation of fragment weighted costs, we also demonstrate that the bi-objective nature (travel and ride time cost) of E-ADARP can be readily handled.

The fragment generation process for E-ADARP follows that of DARP but must additionally satisfy battery-related constraints. Following Rist & Forbes (2021) and Zhao et al. (2025), we compute a tightened time window for each fragment f , defining its feasible departure time index set DT_f .

Using fragments can simplify the bi-objective nature in E-ADARP. To see this, note that node arcs incur no ride time cost, whereas only fragments involve. Consequently, computing the weighted cost of a fragment allows the ride time component of E-ADARP to be incorporated directly. Intuitively, the ride time cost of a fragment may vary across different schedules. However, Su et al. (2024) demonstrate that each fragment is associated with a fixed minimum ride time cost, which can be precomputed by solving a subproblem that enforces all the E-ADARP constraints along the fragment's route (see the Appendix A of Su et al. (2024)). This minimum cost remains unchanged regardless of how the fragment is embedded in a full path. We follow this way to get each fragment's minimum ride time cost. Accordingly, the weighted cost of a fragment equals λ times its travel cost plus $(1 - \lambda)$ times its precomputed minimum ride time cost, where the travel cost is the sum of its constituent arcs. In contrast, the weighted cost of a node arc is simply λ times its travel cost.

The battery-time-space (BTS) fragment-based network $G(N_N, F, A_N)$ for E-ADARP comprises the BTS node set N_N , the BTS fragment set F , and the battery-time-expanded node arc set A_N . The BTS network extends the (physical) fragment-based one (see Section 3.2.1) by incorporating time and battery

dimensions.

The *BTS node* $h \in N_N$ is a tuple consisting of a location $i \in N$, a time index $t \in T$, and a battery index $b \in B$. Specifically, h can be expressed as (i, t, b) . The BTS node set N_N includes the BTS origin depot $O^+ = (0, t_{\min}, b_{\max})$, the BTS destination depot $O^- = (2n + 1, t_{\max}, \gamma b_{\max})$, the BTS pickup nodes, and the BTS delivery nodes. The BTS pickup and delivery nodes correspond to the pickup and delivery locations, with the respective sets denoted by P_N and D_N . All BTS nodes can be generated by assigning each location i with all its feasible time indices $t \in \{tn \in T : e_i \leq tn \leq l_i\}$ and all its feasible battery indices $b \in B$. Here, the origin depot has t_{\min} and b_{\max} as its only feasible time and battery indices, respectively, while the destination depot has t_{\max} and γb_{\max} as its only feasible time and battery indices.

The *BTS fragment* represents a three-dimensional movement, capturing battery consumption, time progression (including waiting time along its physical fragment due to time windows), and physical travel. A BTS fragment f can be expressed as (h, ϕ, h') , where ϕ represents a route path, $h = (i, t, b)$ is a BTS start node, and $h' = (i', t', b')$ is a BTS end node. F is constructed by combining all fragments with various feasible departure times and initial SoCs. A fragment with route path ϕ , physical start node i , physical end node i' , departing time $t \in DT_f$, and initial battery level $b \in B$ (where each fragment may have a subset of battery indices) can be represented in BTS form as $f = ((i, t, b), \phi, (i', t', b'))$. Here, t' equals to the earliest arrival time at i' when a vehicle departs from node i at time t , follows ϕ , and satisfies all the time window and maximum ride time constraints. b' is equal to b minus the total battery consumption of all arcs within ϕ . During creation, the condition $b' \geq b_{\min}$ must hold.

The *battery-time-expanded node arc* can be classified into three types, namely, the *BTS node arc*, the *idle node arc*, and the *charging node arc*. Its set A_N includes all the three types of node arc set. To describe a battery-time-expanded node arc, we use the same format $((i, t, b), \phi, (i', t', b'))$ as in a BTS fragment, where ϕ might denote an arc, a location, or a partial path.

The BTS node arc represents the movement in terms of battery consumption, time progression, and physical travel between two customer locations. The BTS node arc follows the same format as the BTS fragment and its set is constructed in the same way as F . Here, for a BTS node arc ending at O^- , if its generated $b' \geq \gamma b_{\max}$, b' is set to γb_{\max} .

The idle node arc reflects movement solely in the time dimension while maintaining the same SoC and physical location. Its set is generated by assigning each location i with all feasible departure times $t \in T$ and battery SoCs $b \in B$. An idle node arc typically has the format $((i, t, b), i, (i, t', b))$, where $t' \in T$ is the next feasible time index following $t \in T$.

The charging node arc represents movement from a customer location to a charging station and then to another customer location. The charging node arc set is constructed by combining all node arcs with feasible departure time, initial SoCs, final SoCs, and charging stations. If a node arc (i, i') passes through a charging station $s \in S$ and departs at time $t \in T$ with an initial SoC $b \in B$ and a final SoC $b' \in B$, the corresponding charging node arc is represented as $((i, t, b), (i, s, i'), (i', t', b'))$. The earliest arrival time t' is then given by $t' = t + C_{is}^t + C_{si'}^t + \frac{(b' - b) + (C_{is}^t + C_{si'}^t)\beta}{\alpha}$. Here, C_{is}^t and $C_{si'}^t$ denote the travel times from i to s and from s to i' , respectively, while $\frac{(b' - b)}{\alpha}$ and $\frac{(C_{is}^t + C_{si'}^t)\beta}{\alpha}$ represent the recharging time required to increase the SoC from b to b' and the additional recharging time needed to compensate for the energy consumed during the trip. During arc generation, the conditions $b - C_{is}^t\beta \geq b_{\min}$ and $b' + C_{si'}^t\beta \leq b_{\max}$ must hold; for arcs ending at O^- , the condition $b - C_{is}^t\beta \geq \gamma b_{\max}$ must also be satisfied.

A critical consideration is the preselection of charging stations for charging node arcs. In event- or arc-based formulations, where only the physical start and end locations are known (for each arc), intermediate stations close to either location must be retained during preprocessing to ensure battery feasibility—either to enable access to the station from the start node under limited battery, or to allow sufficient battery for reaching the end node after recharging. In contrast, in BTSFF applied to D-E-ADARP, the initial and final SoC levels for each charging node arc are known in advance, enabling direct selection of the least-detour station as long as battery constraints are met. However, in BTSFF applied to E-ADARP, when callbacks are used to ensure optimality, we need to adopt the same preprocessing strategy as the arc-based formulation, as rounding can introduce inaccuracy in the actual pre- and post-charging SoCs. Consequently, multiple charging node arcs with identical BTS start and end nodes but different associated stations may need to be retained. During the callback phase, a lower-cost arc may be eliminated due to battery infeasibility, and a higher-cost alternative may subsequently appear in the feasible solution.

Building on these definitions, the weighted cost of each fragment or battery-time-expanded node arc $f \in F \cup A_N$, denoted by C_f^w , is derived directly from its physical counterpart.

Figure 2 illustrates the relationship between battery SoC and time along a feasible path. In this figure, the horizontal axis represents time, while the vertical axis indicates battery SoC. O^+ and O^- denote the origin and destination depots, respectively. The dark solid lines represent BTS fragments corresponding to the trips from p_1 to d_2 , p_4 to d_4 , and p_7 to d_7 ; if a fragment contains intermediate locations, its route path is labeled above the line (e.g., $p_1 \rightarrow p_2 \rightarrow d_1 \rightarrow d_2$). The dark dashed lines denote BTS node arcs, such as the connections from O^+ to p_1 , from d_2 to p_4 , and from d_7 to O^- . Both BTS fragments and BTS node arcs

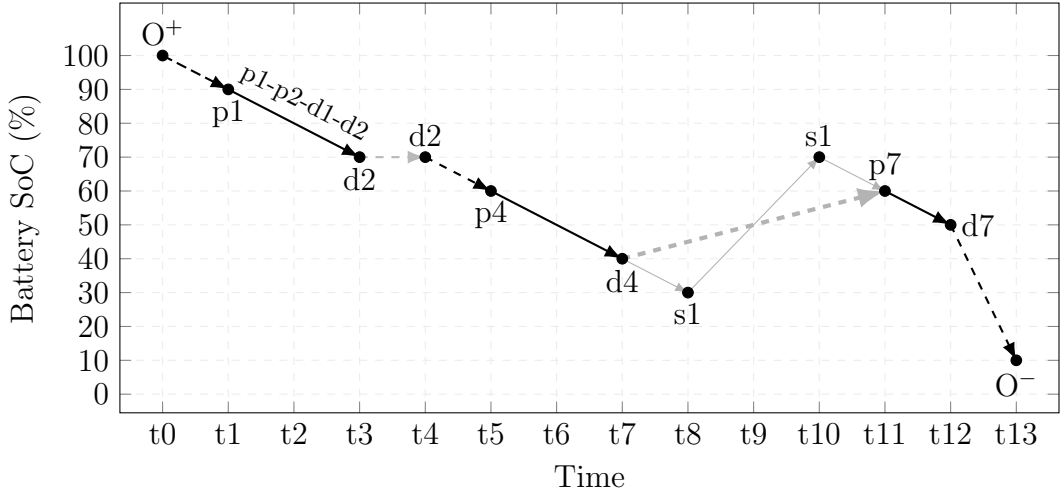


Figure 2: Battery-time relationship in a feasible path

result in a decrease in SoC while the time index increases. The (normal-thickness) gray dashed line corresponds to an idle node arc, indicating the passage of time without changes in both location and SoC (e.g., between two d_2 nodes). Finally, the ultra-thick dashed gray line corresponds to a charging node arc, representing the movement from d_4 to p_7 with an intermediate stop at station s_1 . The detailed route path along this arc is shown as a light gray solid line. Along this arc, the SoC first decreases during travel from d_4 to s_1 (the left one), increases while recharging at s_1 , and then decreases again from s_1 (the right one) to p_7 , while the time index increases continuously due to both travel and charging durations.

3.3 Battery-time-space fragment-based formulation for E-ADARP

We will now formalize the foregoing concepts. We use the notation F_h^+ for the set of BTS fragments starting at BTS node $h \in P_N$, F_h^- for those ending at BTS node $h \in D_N$, and F_i for the set of BTS fragments traversing location $i \in P$. Additionally, A_h^+ and A_h^- represent the set of battery-time-expanded node arcs starting from BTS node $h \in N_N \setminus \{O^-\}$ and the set of battery-time-expanded node arcs ending at BTS node $h \in N_N \setminus \{O^+\}$, respectively.

The problem can then be formulated as follows. The decision variables are summarized in Table 1.

$$\min \quad \sum_{f \in F} C_f^w X_f + \sum_{a \in A_N} C_a^w Y_a \quad (1)$$

Table 1: Decision variables of BTSFF

Decision variables	Definition
X_f	= 1, if the BTS fragment $f \in F$ is traversed; = 0, otherwise
Y_a	= 1, if the battery-time-expanded arc $a \in A_N$ is traversed; = 0, otherwise

$$s.t. \quad \sum_{f \in F_h^-} X_f + \sum_{a \in A_h^-} Y_a = \sum_{f \in F_h^+} X_f + \sum_{a \in A_h^+} Y_a \quad h \in P_N \cup D_N \quad (2)$$

$$\sum_{f \in F_i} X_f = 1 \quad i \in P \quad (3)$$

$$\sum_{a \in A_{O^+}^+} Y_a \leq |V| \quad (4)$$

$$X_f \in \{0, 1\} \quad f \in F \quad (5)$$

$$Y_a \in \{0, 1\} \quad a \in A_N \quad (6)$$

The objective function (1) minimizes the total weighted cost of traversed BTS fragments and battery-time-expanded node arcs. Constraints (2) describe the network flow for the BTS fragments and battery-time-expanded node arcs. This can be divided into two scenarios: network flow at a BTS pickup node belonging to P_N or at a BTS delivery node belonging to D_N , since a BTS fragment can only start at a BTS pickup node and end at a BTS delivery node. Constraints (3) ensure that each pickup location is visited exactly once. Since pairing constraints are already embedded within each fragment, it is not necessary to separately ensure that the delivery location is visited. Constraints (4) state that at most $|V|$ vehicles are used. This is achieved by restricting the number of vehicles traversing the time-expanded node arcs that originate from O^+ . Constraints (5) and (6) specify the domains of X and Y , respectively.

When vehicles have distinct origin nodes (equal in number to the fleet size), denoted by the set O_v^+ , and multiple potential destination nodes—possibly exceeding the fleet size—denoted by the set D_v^- , constraints (7) and (8) replace constraint (4), consistent with the formulation of Bongiovanni et al. (2019); Su et al. (2024).

$$\sum_{a \in A_i^+} Y_a = 1 \quad i \in Ov^+ \quad (7)$$

$$\sum_{a \in A_i^-} Y_a \leq 1 \quad i \in Dv^+ \quad (8)$$

3.4 Battery swapping variant of E-ADARP

The battery swapping variant of E-ADARP is denoted as E-ADARP-BS. Compared to E-ADARP, E-ADARP-BS assumes that upon arriving at a charging station, the vehicle’s SoC is instantly restored to full capacity (equal to b_{\max}), subject to a fixed battery swapping time T_{bs} . In contrast to E-ADARP, where partial charging introduces SoC dependencies before and after each charging station and requires linearly increasing recharging time calculations, E-ADARP-BS assumes full recharging with a fixed duration, thereby avoiding the linear recharging time calculations and simplifying time scheduling. Additionally, E-ADARP-BS does not require the consideration of the minimum SoC threshold upon returning to the depot, since battery swapping is sufficiently rapid to ensure a fully charged battery.

We adopt a continuous-time setting while keeping the battery index discretized. We now clarify two points: why only the time dimension is extended to continuous values, and why this setting is applied to E-ADARP-BS but not to E-ADARP. First, although both the battery and time dimensions could, in principle, be corrected via callbacks in BTSFF, handling a continuous battery index would require substantial additional effort. In the time dimension, time windows typically provide waiting time as a buffer, so callbacks are rarely triggered. By contrast, the battery dimension lacks such flexibility, making callbacks almost unavoidable and particularly burdensome. Second, in E-ADARP, linearly increasing recharging times couple the time and battery dimensions, whereas in E-ADARP-BS the fixed swapping duration at each station allows time scheduling to be treated independently of the battery dimension. Our preprocessing, tailored to E-ADARP-BS, further supports this approach: to reduce computation, we incorporate the fixed swapping duration into the travel time from each charging station to all subsequent locations.

In terms of the solution method, BTSFF can be directly applied to this problem with only minor modifications to the BTS network. Specifically, when generating charging node arcs, the recharging time is set to zero and the final SoC is set to full capacity. Callbacks are then required to support BTSFF in correcting rounding inaccuracies, as detailed in Section 4.

4 Extension of BTSFF to E-ADARP and E-ADARP-BS

This section first introduces an exact framework that integrates BTSFF with lazy-constraint callbacks to solve E-ADARP and E-ADARP-BS. We then describe an alternative use of BTSFF for generating valid lower bounds for E-ADARP.

Finally, we present the implementation details of lazy-constraint callbacks for E-ADARP-BS. The framework (formulation plus callback) is adapted from Rist & Forbes (2021), who apply it to DARP rather than to E-ADARP. In addition, unlike their work, we emphasize that the formulation, BTSFF, can itself serve as an efficient lower bound.

We now present the exact framework. First, a relaxed BTS fragment-based network is constructed. Since battery and time are continuous parameters, their consumption along all arcs (and fragments) must be discretized and rounded to predefined feasible levels. During network construction, each BTS fragment or BTS node arc is assigned a discrete time index as the departure time and a pre-defined SoC level as the initial battery state. The corresponding arrival time t' is then rounded down to the nearest $t \in T$, and the final battery level b' is rounded up to the nearest $b \in B$. For each BTS fragment or BTS node arc, the departure time and initial battery level uniquely determine both the arrival time and the final battery level. In contrast, the construction of charging node arcs is more involved. In addition to the departure time and initial battery level, the final battery level b' and the associated charging station must also be known in advance. Based on this information, the required charging duration can be computed to determine the arrival time t' , which is then rounded down to the nearest $t \in T$.

Over the relaxed network, BTSFF would yield both feasible and infeasible solutions with respect to the original problem, as the time and battery consumption on all arcs are effectively underestimated in the constructed network. It can be foreseen that all feasible solutions of the original problem are preserved. However, some infeasible solutions—those that violate certain constraints under the original continuous parameters but satisfy all constraints under the discrete approximation—may also appear. In a minimization problem, such infeasible solutions would be considered only if they incur a lower cost. Therefore, the discretized version can be viewed as a relaxed problem, whose optimal objective value is guaranteed to be less than or equal to that of the original problem, thereby providing a valid lower bound.

Second, lazy-constraint callbacks are incorporated to compensate for the relaxed network. In contrast to the DARP in Rist & Forbes (2021), where subtour elimination, time window, and maximum ride time constraints are enforced through lazy constraints, our approach only focuses on time window constraints. Maximum ride time constraints for customers are already enforced during fragment generation, and the sufficiently fine battery discretization adopted in this study eliminates the need for subtour elimination.

For E-ADARP, given the substantial callback burden, we employ BTSFF in an alternative way—generating valid lower bounds. Computational results in Section 5 will further illustrate its effectiveness.

For E-ADARP-BS, we apply the exact framework. Since the battery dimension in E-ADARP-BS is treated as a discretized input, lazy constraints are imposed only on the time dimension. The implementation follows Rist & Forbes (2021) and is detailed below. As long as we encounter an incumbent solution in the branch-and-bound tree, we create chains. Here, we focus solely on the physical information, without considering time and battery aspects. A *chain* is a sequence of fragments (f_1, \dots, f_c) with a fragment count of $c > 1$, along with $c-1$ node arcs (a_1, \dots, a_{c-1}) connecting them. The start node and the end node of a_i correspond to the end node of fragment f_i and the start node of f_{i+1} , respectively, for $1 \leq i \leq c-1$. If we obtain a chain, we connect its initial and final fragments to the origin and destination depots, respectively, to infer a physical path. After that, we establish a valid time schedule for the path, following all the constraints of E-ADARP-BS. If no valid schedule can be found, the chain is considered infeasible and then be eliminated by constraints (9) ensuring the total count of the BTS fragments and battery-time-expanded node arcs in such a chain does not exceed $2c - 2$. In these constraints, F^f denotes the set of all BTS fragments derived from the physical fragment f , while A_N^a denotes the set of all battery-time-expanded node arcs derived from the physical node arc a .

$$\sum_{f \in F^{f_k}} \sum_{k=1}^c X_f + \sum_{a \in A_N^{a_k}} \sum_{k=1}^{c-1} Y_a \leq 2c - 2 \quad (9)$$

5 Computational results

5.1 Test instances

To evaluate the computational efficiency of different formulations and fragment sets, we employ the benchmark instances commonly used in E-ADARP studies (Bongiovanni et al., 2019; Su et al., 2024; Stallhofer & Parragh, 2025). The instances are categorized into three types: a, r, and u. type-a and type-r are both adapted from classical DARP datasets (Cordeau, 2006; Ropke & Cordeau, 2009), differing primarily in problem scale. Each instance assumes unit demand and a vehicle capacity of three. Type-a instances (14 in total) involve 2-5 vehicles and 16-50 user requests, whereas type-r instances (10 in total) comprise 5-8 vehicles and 60-96 requests. All vehicles start with a full battery of 16.5 kWh, the maximum battery capacity, corresponding to a driving range of 5 hours. They must retain at least 10% of full capacity at all times (thus yielding an effective capacity of 14.85 kWh). Both charging and discharging rates (previously denoted α and β) are set to 0.055 kWh/min, corresponding to a total driving

time of 270 minutes. Type-u instances (14 in total) are generated from an Uber dataset by Bongiovanni et al. (2019). Similar to type-a, they involve 2-5 vehicles and 16-50 requests. The effective battery capacity is set to 3.5 kWh, with charging and discharging rates of 0.055 and 0.0715 kWh/min, respectively, corresponding to approximately 50 minutes of driving time. Across all instance types, a minimum battery level (previously denoted γ , relative to the effective battery capacity) of 10%, 40%, or 70% is imposed before returning to the depot. Public access to these instances is provided by Cordeau (2006) at <http://neumann.hec.ca/chairedistributique/data/darp/branch-and-cut/> and by Bongiovanni et al. (2019).

5.2 Experimental settings, benchmarks, and implementation details

To evaluate the performance of BTSFF across E-ADARP and its variants, we design three experimental settings based on the benchmark instances. These experiments evaluate the effectiveness of BTSFF. As discussed in Section 3, we only consider the setting $N_{\max} = \infty$. A brief summary of the experiments is provided in Table 2, with details explained below.

Table 2: Experiment design for different problem variants

Problem	Benchmarks	BTSFF's purpose	Discretized aspect	Instance type and granularity (min)	γ	Battery capacity
E-ADARP	REBF, Su et al.	LB	Time, battery	a: 5 or 10; u: 2; r: 10	10%, 40%, 70%; 0%	100%, 50%
D-EADARP	REBF	Optimality	Time, battery	a: 5	10%, 40%, 70%	100%, 50%
E-ADARP-BS	REBF	Optimality	Battery only	a: 3; u: 1; r: 5	0%	50%

¹ Full effective battery capacity (expressed in minutes of driving consumption): 270 for types a and r, and 50 for type u. REBF refers to our replication of the event-based formulation of Stallhofer & Parragh (2025). For all three problems, $N_{\max} = \infty$.

An important consideration is the discretization of time and battery. Here, battery units are defined by the driving time required to deplete the corresponding amount of energy, and the granularity is set in proportion to battery capacity. Although different types of instances are considered, we generally use two discretization levels—around 4% and 2% of battery capacity. Specifically, for type-a and type-r instances, under a 24-hour planning horizon and a 5-hour battery capacity, we set the granularity to 10 (or 5) minutes, which yields 144 (or 288) time indices and 27 (or 54) battery levels, with one unit representing approximately 3.7% (or 1.85%) of battery capacity. For type-u instances, under a 200-minute planning horizon and a battery capacity of about 50 minutes, we set the granularity to 2 (or 1) minutes, which yields 100 (or 200) time indices and 25 (or 50)

battery levels, with one unit corresponding to about 4% (or 2%) of capacity. As noted in Section 2.2, these settings ensure a reasonable level of accuracy for routing problems.

The first experiment is designed to assess both the quality of the lower bound generated by BTSFF and its computational efficiency for E-ADARP. In this setting, the original instances remain unchanged. We use a 10-minute granularity for type-a and type-r instances, and a 2-minute granularity for type-u. For further analysis, we also test a 5-minute granularity for type-a. Experiments are conducted under $\gamma \in \{10\%, 40\%, 70\%\}$. Since the $\gamma = 10\%$ scenario automatically serves as a lower bound for $\gamma = 40\%$ and $\gamma = 70\%$, we additionally examine the case with 50% battery capacity and $\gamma = 0\%$ on type-r instances to assess whether BTSFF remains useful for generating lower bounds. We choose a 50% capacity for this test because, with 100% capacity and $\gamma = 0\%$, recharging is rarely required for these instances.

The second experiment aims to evaluate the computational performance of BTSFF in solving D-E-ADARP to optimality. The test instances are adapted from existing benchmark instances to reflect the discretized problem setting. Specifically, all travel times, battery consumptions, earliest departure times, and latest arrival times are rounded to the nearest multiple based on the chosen granularity. Maximum ride times—which, as previously noted, include both the original ride time and the implicitly handled service time—are rounded up to align with the time granularity. This upward rounding ensures instance feasibility, though it increases solving difficulty due to the expanded solution space. This setup is not intended to approximate E-ADARP, but to generate discretized instances that yield identical objective values when solved by BTSFF and other continuous-parameter models, thereby enabling a fair comparison. In this experiment, a 5-minute granularity is used, and all γ values are considered. Importantly, the first experiment rounds after fragment generation, while the second rounds arc parameters before generating fragments.

The third experiment aims to evaluate the computational performance of an exact algorithm framework, composed of BTSFF and a callback mechanism, for solving E-ADARP-BS. In this setting, instances are adapted from benchmark datasets by retaining continuous time parameters while rounding arc battery consumptions. We use battery granularities of 3 minutes for type-a, 1 minute for type-u, and 5 minutes for type-r instances. For the time dimension, we adopt a coarser granularity of 50 minutes and rely primarily on callbacks to correct time inaccuracies. As this problem is a special case of E-ADARP without partial charging, the time and battery dimensions are decoupled. Thus, we adopt finer battery granularities to better demonstrate the potential of BTSFF. In E-ADARP-BS, since γ is not required and the default battery capacity suffices for most instances with-

out recharging, we examine reduced capacities of 50% of the original, typically inducing two to three recharging operations per route.

For benchmarks across all three experiments, we consider Stallhofer & Parragh (2025) and Su et al. (2024). As the first benchmark, we replicate the event-based formulation of Stallhofer & Parragh (2025) (REBF), adopting Cuts 1, 4, 6, and 7 from their study. We believe our replication procedure is convincing, as our results for E-ADARP with $N_{\max} = 1$ (see Appendix A of the Online Supplementary Material) generally surpass the reported ones, particularly for medium and large instances. This improvement may be attributable to the use of solver Gurobi rather than CPLEX, as also suggested by the team of Stallhofer & Parragh (2025). Consequently, for our three experiments of E-ADARP with $N_{\max} = \infty$, we use the replicated procedure as the benchmark. The event-based formulation requires replicating charging stations up to N_{\max} times when $N_{\max} > 1$. Since each station is typically visited 2–4 times for type-a and type-u instances and 4–8 times for type-r instances, we set $N_{\max} = 5$ for type-a and type-u, and $N_{\max} = 10$ for type-r instances. For cases with 50% battery capacity, N_{\max} is further augmented by 5. As the second benchmark, we use the B&P algorithm results of Su et al. (2024) with $N_{\max} = \infty$. We report only the results provided in Su et al. (2024), without further replication on new test cases, since REBF already performs better than their reported results (see Appendix A of the Online Supplementary Material for $\gamma = 1$ and Table 3 for $\gamma = \infty$).

In evaluating computational performance, we report several indicators for BTSFF and REBF: the solver CPU time (CPU), the total runtime (*Time*), the best-found objective value (OBJ), the best-known lower bound (LB), and the optimality gap (Gap), all measured under a 30-minute limit. Here, $\text{Gap} = \frac{\text{OBJ} - \text{LB}}{\text{OBJ}} * 100\%$. As the number of test instances is large, we adopt a 30-minute limit for BTSFF and REBF. We also include results from Su et al. (2024), with 2-hour limits for types a and u and 5 hours for type-r. Although the runtime settings differ, the 30-minute results of BTSFF already provide sufficiently high-quality solutions to support convincing conclusions. For BTSFF, we additionally report the number of fragments ($|F|$), the fragment generation time (F-time), and the BTS network construction time (Net). All time values in the following tables are reported in seconds.

All our algorithms (BTSFF and REBF) are implemented using the Python programming language. Experiments were run on a Windows 11 Pro (64-bit) system with a 13th Gen Intel Core i7-1365U CPU @ 1.80 GHz and 32 GB RAM. All linear formulations are solved with the commercial solver Gurobi 11.0.3 with a single thread; all other Gurobi parameters are set to their default values.

5.3 Lower Bound of E-ADARP

To evaluate the quality of lower bounds in E-ADARP, we introduce two additional indicators, $Diff_{RE}$ and $Diff_{Su}$, defined as the relative percentage difference between the LB of BTSFF and that of REBF, and the relative percentage difference between the LB of BTSFF and that of Su et al. (2024), respectively. These metrics are designed to assess the quality of the proposed lower bound for the original problem, as obtained by BTSFF over a relaxed network. Since E-ADARP is a minimization problem, a positive value (of $Diff_{RE}$ or $Diff_{Su}$) indicates that the LB from BTSFF is better (or higher), whereas a negative value indicates that the obtained LB is worse.

Table 3: Average computational performance of different algorithms on E-ADARP with $N_{\max} = \infty$

Battery	Granularity	Type	γ	BTSFF (relaxed)			REBF			Results of Su et al.		
				CPU	Time	Gap	Time	Gap	$Diff_{RE}$	Time	Gap	$Diff_{Su}$
100%	10 min	a	10%	6.4	34.0	0.00%	64.2	0.00%	-0.18%	Not reported		
			40%	6.5	33.0	0.00%	90.7	0.00%	-0.23%	910.3	0.00%	-0.23%
			70%	4.8	34.3	0.00%	1018.5	0.32%	-0.62%	1795.3	0.30%	-0.92%
	5 min	a	10%	54.5	141.2	0.00%	-0.13%			Same above		
			40%	52.8	143.8	0.00%	-0.17%			Same above		
			70%	63.4	153.8	0.00%	-0.40%			-0.18%		
	2 min	u	10%	104.2	149.6	0.00%	209.6	0.04%	-0.26%	1873.6	0.03%	-0.27%
			40%	109.9	163.3	0.00%	251.9	0.05%	-0.39%	1792.3	0.03%	-0.43%
			70%	113.6	167.9	0.00%	571.7	0.22%	-0.77%	3096.7	0.27%	-0.78%
	10 min	r	10%	90.9	312.2	0.00%	1128.7	0.55%	0.32%	9446.8	-0.33%	2.91%
			40%	108.2	314.0	0.00%	1298.8	0.68%	0.38%	10355.6	-0.69%	1.59%
			70%	99.3	303.5	0.00%	1800.0	1.83%	0.74%	13289.3	-1.96%	4.43%
50%	10 min	r	0%	27.3	172.7	0.00%	1437.0	1.81%	0.54%	Not reported		

¹ Battery: battery capacity. Type: instance type. BTSFF (relaxed): BTSFF solves a relaxed version of E-ADARP, yielding a valid lower bound, whereas REBF and Su et al. address E-ADARP directly. Discretization granularity affects only BTSFF’s performance.

Table 3 summarizes the average computational results of BTSFF, REBF, and Su et al. (2024) for E-ADARP under $N_{\max} = \infty$, while the complete set of detailed results is provided in Appendix B of the Online Supplementary Material. Note that BTSFF actually solves a relaxed problem to optimality, and its LB (or OBJ) serves as a lower bound for the original problem.

The key finding from Table 3 is that BTSFF generates high-quality lower bounds for E-ADARP with substantially shorter runtimes. In particular, the last four rows for large-size instances (type-r) show positive values in the $Diff_{RE}$ and $Diff_{Su}$ columns, indicating that BTSFF provides stronger bounds than existing algorithms. Meanwhile, BTSFF achieves runtime reductions of about one order of magnitude compared with REBF and up to two orders of magnitude compared

with Su et al. (2024). Furthermore, the first nine rows of results reveal that for small-size instances (type-a and type-u), the lower bounds are slightly weaker than those of the benchmarks, primarily because these instances are nearly solved to optimality (see the Gap column in REBF and the results of Su et al.). Nevertheless, this also demonstrates the high quality of our lower bounds.

Moreover, the results for type-a instances with different granularities (see the first six rows) indicate that the runtime of BTSFF is strongly influenced by the choice of granularity. Smaller granularities lead to denser networks, which in turn require more CPU time and longer network construction time (computed as total runtime minus CPU time). At the same time, as shown in the $Diff_{RE}$ and $Diff_{Su}$ columns, finer granularities yield higher values, corresponding to stronger lower bounds.

Additionally, Table 3 clarifies a potential concern: while scenarios with lower γ (requiring less runtime) may serve as lower bounds for higher values, this does not reduce the value of BTSFF in providing valid lower bounds. First, runtimes across different γ values for the same instance type in BTSFF are comparable, and even the $\gamma = 70\%$ case in BTSFF is faster than the $\gamma = 10\%$ case in REBF (the fastest for that instance type). Second, our supplementary test with 50% battery capacity and $\gamma = 0\%$ (see the last row)—a setting that enforces recharging, unlike the near non-recharging case of 100% capacity—demonstrates that BTSFF also serves as a good-quality lower bound for low- γ scenarios.

5.4 Computational performance of D-E-ADARP

Table 4: Average computational performance of different algorithms on E-ADARP with $N_{\max} = \infty$

		BTSFF			REBF	
Battery	γ	CPU	Time	Gap	Time	Gap
100%	10%	105.7	236.1	0.00%	76.0	0.00%
	40%	108.2	244.8	0.00%	225.6	0.00%
	70%	125.1	261.9	0.00%	1126.4	0.52%
50%	10%	46.2	109.0	0.00%	927.7	0.33%
	40%	54.9	118.9	0.00%	1258.1	0.79%
	70%	42.7	102.7	0.00%	1780.5	1.83%

¹ Battery: battery capacity.

Table 4 reports the average computational performance of BTSFF and REBF on type-a instances of D-E-ADARP under a 5-minute granularity with $N_{\max} = \infty$, with detailed results given in Appendix C of the Online Supplementary Material.

The results show that BTSFF outperforms REBF when $\gamma = 70\%$, where recharging is relatively more frequent, but performs worse when $\gamma = 10\%$, where recharging is rare. Moreover, the runtime of BTSFF remains nearly constant across different γ values, whereas the runtime of REBF increases substantially as γ grows. This highlights the advantage of BTSFF under higher γ values. In addition, when the battery capacity is reduced to 50%, even the $\gamma = 10\%$ case—the easiest to solve—becomes challenging for REBF, as the reduced battery size necessitates recharging and thereby complicates computation. In this setting, BTSFF performs even better than with 100% capacity because fewer battery indices result in a smaller BTS network.

An additional remark pertains to the order of rounding and fragment generation. In the current experiment, all arc-based parameters are first rounded and then used to create fragments, which increases both rounding error and fragment count. For the same instance, Table 4 (rows 1–3, with 5-minute granularity applied before fragment generation) reports longer runtimes than Table 3 (rows 4–6, with 5-minute granularity applied after fragment generation) for type-a instances, and Table C.1 in the Online Supplementary Material shows a higher number of fragments than Table B.2. One contributing factor, as noted in Section 5.2, is the rounding up of the maximum ride time; however, much of the effect stems from the overall rounding procedure. This can be illustrated by a simple example: under continuous time, if the arrival times at the end node of two fragments are 29.9 and 30.1 with a latest feasible arrival time of 30, only the first is feasible, whereas the second becomes feasible if the time is discretized in advance. In contrast, if fragments are generated and selected under continuous-time parameters and only then rounded, the number of fragments does not increase and the rounding error per fragment remains small. In this case, the computational difficulty would be comparable to that in Table 3 of Section 5.3, with the only difference being that time is rounded rather than rounded down. Here, we round arc-based parameters in this experiment to create identical instances for both BTSFF and REBF, to ensure a fair comparison. We then restrict our evaluation to type-a instances only, rather than conducting detailed comparisons across all instance types.

5.5 Computational performance of E-ADARP-BS

Table 5: Computational performance of different algorithms on E-ADARP-BS with $N_{\max} = \infty$

		BTSFF							REBF						
B-unit	Name	F	F-time	Net	CPU	Time	OBJ	LB	Gap	CPU	Time	OBJ	LB	Gap	
3 min	a2-16	32	1.5	5.0	0.9	7.9	237.40	237.40	0.00%	7.1	7.3	237.40	237.40	0.00%	
	a2-20	50	0.2	2.6	1.2	4.4	279.99	279.99	0.00%	22.3	22.6	279.99	279.99	0.00%	
	a2-24	64	0.1	2.6	5.6	8.9	346.99	346.99	0.00%	64.6	65.1	346.99	346.99	0.00%	
	a3-18	65	0.3	2.1	0.8	3.6	237.75	237.75	0.00%	13.8	14.0	237.75	237.75	0.00%	
	a3-24	106	0.6	4.4	11.5	17.6	275.10	275.10	0.00%	29.8	30.4	275.10	275.10	0.00%	
	a3-30	89	0.4	6.3	13.9	22.8	413.36	413.36	0.00%	1799.3	1800.0	413.36	412.24	0.27%	
	a3-36	116	0.5	9.3	144.2	157.3	483.34	483.34	0.00%	1798.6	1800.0	484.27	472.60	2.41%	
	a4-16	82	0.2	1.8	1.1	3.2	222.49	222.49	0.00%	1.9	2.1	222.49	222.49	0.00%	
	a4-24	95	0.5	4.8	2.9	9.1	311.03	311.03	0.00%	9.8	11.0	311.03	311.03	0.00%	
	a4-32	239	1.4	6.9	20.0	30.4	395.10	395.10	0.00%	223.4	224.4	395.10	395.10	0.00%	
1 min	a4-40	239	1.7	13.5	51.0	70.7	455.83	455.83	0.00%	504.1	506.3	455.83	455.83	0.00%	
	a4-48	346	0.9	12.9	164.1	184.1	555.74	555.74	0.00%	938.2	950.1	555.74	555.74	0.00%	
	a5-40	319	1.0	11.9	39.2	56.4	414.50	414.50	0.00%	52.3	56.8	414.50	414.50	0.00%	
	a5-50	692	2.7	18.6	159.3	189.1	561.84	561.84	0.00%	148.2	162.7	561.84	561.84	0.00%	
	Avg						44.0	54.7	0.00%			403.8		0.19%	
	u2-16	60	0.8	1.5	4.5	7.2	58.54	58.54	0.00%	33.8	34.2	58.54	58.54	0.00%	
	u2-20	168	0.9	2.1	11.1	14.8	56.95	56.95	0.00%	122.1	123.4	56.95	56.95	0.00%	
	u2-24	66	0.3	2.4	8.2	12.2	91.58	91.58	0.00%	272.8	273.4	91.58	91.58	0.00%	
	u3-18	78	0.4	1.5	2.8	5.2	51.43	51.43	0.00%	99.7	100.2	51.43	51.43	0.00%	
	u3-24	130	0.7	2.8	12.3	16.6	68.22	68.22	0.00%	87.3	88.4	68.22	68.22	0.00%	
1 min	u3-30	182	2.3	4.2	115.7	124.7	77.98	77.98	0.00%	1798.4	1800.0	77.98	75.98	2.56%	
	u3-36	223	0.7	3.5	32.6	38.1	105.59	105.59	0.00%	1796.9	1800.0	106.12	103.44	2.52%	
	u4-16	74	0.3	1.5	1.2	3.6	54.61	54.61	0.00%	5.3	5.8	54.61	54.61	0.00%	
	u4-24	57	0.2	2.9	4.2	8.4	90.81	90.81	0.00%	45.3	45.9	90.81	90.81	0.00%	
	u4-32	174	0.9	3.9	27.5	34.1	100.64	100.64	0.00%	600.6	611.9	100.64	100.64	0.00%	
	u4-40	144	0.6	7.3	36.8	47.0	136.88	136.88	0.00%	1797.8	1800.0	136.90	134.32	1.88%	
	u4-48	922	8.0	9.5	319.3	341.0	149.39	149.39	0.00%	1788.1	1800.0	149.39	144.75	3.11%	
	u5-40	330	0.8	4.4	30.7	37.4	124.33	124.33	0.00%	1795.1	1800.0	124.33	123.11	0.98%	
	u5-50	548	6.4	11.9	87.5	110.4	145.20	145.20	0.00%	1787.9	1800.0	145.20	144.01	0.81%	
	Avg						49.6	57.2	0.00%			863.1		0.85%	
5 min	r5-60	734	9.6	17.8	128.3	161.5	689.89	689.89	0.00%	1749.5	1800.0	689.89	685.98	0.57%	
	r6-48	11048	45.9	9.0	7.8	66.2	507.01	507.01	0.00%	132.1	143.1	507.01	507.01	0.00%	
	r6-60	879	3.4	10.2	278.9	297.0	691.82	691.82	0.00%	1752.4	1800.0	692.40	690.36	0.29%	
	r6-72	1442	21.3	14.5	45.3	89.1	763.52	763.52	0.00%	1742.0	1800.0	764.32	758.53	0.76%	
	r7-56	1589	6.5	11.1	22.1	43.6	612.56	612.56	0.00%	1139.9	1193.1	612.56	612.50	0.00%	
	r7-70	2636	16.4	14.1	98.4	136.0	756.03	756.03	0.00%	1753.7	1800.0	756.03	741.72	1.89%	
	r7-84	5221	57.4	21.2	1709.0	1800.0	901.37	875.07	2.92%	1724.2	1800.0	882.62	858.89	2.69%	
	r8-64	47593	527.6	26.3	35.9	597.1	632.53	632.49	0.00%	524.7	566.8	632.53	632.53	0.00%	
	r8-80	17180	243.3	24.4	107.8	386.0	791.89	791.89	0.00%	1714.9	1800.0	791.89	787.69	0.53%	
	r8-96	4899	36.8	30.6	1716.4	1800.0	1141.31	1022.28	10.43%	1621.3	1800.0	1041.14	995.28	4.40%	
	Avg						415.0	537.6	1.33%			1450.3		1.11%	

¹ B-Unit: battery granularity. Name: the initial letter denotes the instance type.

Table 5 reports the computational results of BTSFF and REBF for E-ADARP-BS under $N_{\max} = \infty$. In this case, time is treated as a continuous input, whereas the discretized battery granularity is indicated in the table. Table 5 shows that for solving E-ADARP-BS, BTSFF outperforms REBF for all types of instances in terms of both solution quality and computational time. For type-u instances, BTSFF requires less runtime but exhibits slightly larger optimality gaps. This is mainly attributed to the last instance (r8-96), where a particularly large gap

inflates the average. However, for the instance of r8-96, when the time limit is extended to two hours, the resulting gaps are reduced to 0.15% for BTSFF and 1.66% for REBF, respectively.

6 Conclusions

This study is motivated by practical scenarios in which time and battery parameters are naturally represented in a coarse form. Building on this motivation, we define a discrete variant of the Electric Autonomous Dial-a-Ride Problem to better capture such settings. To better address this problem, we propose a battery-time-space fragment-based formulation that extends the traditional fragment-based method—originally defined in physical space—into a battery-time-space network. Beyond its application to the discrete version of the problem, the proposed formulation also generates high-quality lower bounds for the original problem with continuous parameters. Furthermore, we integrate the formulation with a callback mechanism to develop an exact solution framework for a problem variant involving battery swapping. Computational results demonstrate that, under reasonable time and battery granularities, BTSFF efficiently solves the discrete version of the problem, provides tight lower bounds for the original problem, and accelerates the solution process for the battery swapping variant. These findings underscore the potential of BTSFF as an effective framework for this class of problems.

Although the formulation is built on a three-dimensional network with a large number of variables, it demonstrates strong computational performance, likely due to its underlying network flow structure. An additional advantage is its scalability with respect to the number of charging stations (for D-E-ADARP): the variable count remains stable because each charging node arc preselects the lowest-cost feasible station. In contrast, event-based and B&P methods typically retain multiple candidate stations per arc, as their preprocessing relies on broader criteria beyond detour cost. A limitation of fragments lies in the treatment of time windows. When time windows are relaxed, the number of fragments can increase accordingly. In such cases, switching to restricted fragments—subdivisions of fragments—offers a viable alternative. We adopt the current fragment because existing studies on E-ADARP, such as Su et al. (2024), indicate that relatively tight time windows are more common in such problems and report that the number of enumerated fragments remains quite limited.

References

Alyasiry, A. M., Forbes, M., & Bulmer, M. (2019). An exact algorithm for the pickup and delivery problem with time windows and last-in-first-out loading. *Transportation Science*, 53, 1695–1705. doi:10.1287/trsc.2019.0905.

Baldacci, R., Bartolini, E., & Mingozzi, A. (2011). An Exact Algorithm for the Pickup and Delivery Problem with Time Windows. *Operations Research*, 59, 414–426. doi:10.1287/opre.1100.0881.

Bongiovanni, C., Kaspi, M., & Geroliminis, N. (2019). The electric autonomous dial-a-ride problem. *Transportation Research Part B: Methodological*, 122, 436–456. doi:10.1016/j.trb.2019.03.004.

Bruni, M. E., Cubillos, M., & Jabali, O. (2025). Layered Graph Models for the Electric Vehicle Routing Problem With Nonlinear Charging Functions. *Networks*, 85, 113–126. doi:10.1002/net.22251.

BYD Auto (2025). BYD Unveils Super e-Platform with Megawatt Flash Charging for Electric Vehicles, Matching Refueling Speeds. URL: <https://www.byd.com/mea/news-list/byd-unveils-super-e-platform-with-megawatt-flash-charging>.

Cordeau, J.-F. (2006). A Branch-and-Cut Algorithm for the Dial-a-Ride Problem. *Operations Research*, 54, 573–586. doi:10.1287/opre.1060.0283.

Fernández, E., Leitner, M., Ljubić, I., & Ruthmair, M. (2022). Arc Routing with Electric Vehicles: Dynamic Charging and Speed-Dependent Energy Consumption. *Transportation Science*, 56, 1219–1237. doi:10.1287/trsc.2022.1126.

Gaul, D., Klamroth, K., Pfeiffer, C., Stiglmayr, M., & Schulz, A. (2024). A tight formulation for the dial-a-ride problem. *European Journal of Operational Research*, (pp. 1–20). doi:10.1016/j.ejor.2024.09.028.

Gaul, D., Klamroth, K., & Stiglmayr, M. (2022). Event-based MILP models for ridepooling applications. *European Journal of Operational Research*, 301, 1048–1063. doi:10.1016/j.ejor.2021.11.053.

Mahmoudi, M., & Zhou, X. (2016). Finding optimal solutions for vehicle routing problem with pickup and delivery services with time windows: A dynamic programming approach based on state-space-time network representations. *Transportation Research Part B: Methodological*, 89, 19–42. doi:10.1016/j.trb.2016.03.009.

Rist, Y., & Forbes, M. (2022). A column generation and Combinatorial Benders Decomposition algorithm for the Selective Dial-A-Ride-Problem. *Computers and Operations Research*, 140, 105649. doi:10.1016/j.cor.2021.105649.

Rist, Y., & Forbes, M. A. (2021). A New Formulation for the Dial-a-Ride Problem. *Transportation Science*, 55, 1113–1135. doi:10.1287/trsc.2021.1044.

Ropke, S., & Cordeau, J.-F. (2009). Branch and Cut and Price for the Pickup and Delivery Problem with Time Windows. *Transportation Science*, 43, 267–286. doi:10.1287/trsc.1090.0272.

Santini, A., Plum, C. E. M., & Ropke, S. (2018). A branch-and-price approach to the feeder network design problem. *European Journal of Operational Research*, 264, 607–622. doi:doi.org/10.1016/j.ejor.2017.06.063.

Stallhofer, V., & Parragh, S. N. (2025). Event-based models for the electric autonomous dial-a-ride problem. *Transportation Research Part C: Emerging Technologies*, 171, 104896. doi:10.1016/j.trc.2024.104896.

Su, Y., Dupin, N., Parragh, S. N., & Puchinger, J. (2024). A Branch-and-Price algorithm for the electric autonomous Dial-A-Ride Problem. *Transportation Research Part B: Methodological*, 186, 103011. doi:10.1016/j.trb.2024.103011.

Su, Y., Dupin, N., & Puchinger, J. (2023). A deterministic annealing local search for the electric autonomous dial-a-ride problem. *European Journal of Operational Research*, 309, 1091–1111. doi:10.1016/j.ejor.2023.02.012.

Zhang, W., Jacquillat, A., Wang, K., & Wang, S. (2023). Routing Optimization with Vehicle–Customer Coordination. *Management Science*, 69, 6876–6897. doi:10.1287/mnsc.2023.4739.

Zhao, B., Wang, K., Wei, W., & Leus, R. (2025). The dial-a-ride problem with limited pickups per trip. *European Journal of Operational Research*, 327, 776–790. doi:10.1016/j.ejor.2025.05.051.